In Situ Fracture Observations on Tempered Martensite Embrittlement in an AISI 4340 Steel

B.C. KIM, S. LEE, D.Y. LEE, and N.J. KIM

The ability to document and understand the micromechanics of fracture processes, especially as they relate to macroscopic failure mechanisms, along with the influence of chemistry, microstructure, and processing, now underlies a good deal of alloy design methodology. Recent advances in fracture mechanics, in particular for ductile alloys, have provided new means of studying the interaction of cracks moving under quasi-static conditions in various microstructures. A particularly interesting set of recent studies of this type has shown, for example, that when ultrahigh-strength steels, such as AISI 4340 steels, are tempered near 350 °C, a loss in toughness, called tempered martensite embrittlement (TME), is observed. This is usually characterized by a trough in the plot of Charpy impact energy as a function of tempering temperature and by the ductile-brittle transition temperature exhibiting a maximum at the temperature corresponding to the minimum in the Charpy toughness.[1-6] Since this embrittlement problem in the 4340 steel limits the service temperature of the steel, it is very important to identity the reason of the problem for the development of ultrahigh-strength steels with improved toughness.

Attempts to explain the TME phenomenon have focused on the possible effects of carbide distributions and segregation of impurity elements on prior austenite grain boundaries as key metallurgical variables. Thomas and co-workers[1,3] have suggested a mechanism of TME in which the drop in toughness can be correlated with the decomposition of lath-boundary retained austenite and the subsequent formation of interlath cementite films during tempering. These interlath carbides may provide crack nucleation sites or easy crack paths. Recently, the effects of impurity content and grain size on the percentage of intergranular fracture in high-strength steels tempered in the TME range have been discussed. Several researchers[4,5,6] have found that impurity elements, primarily phosphorus and sulfur, segregate to the grain boundaries during austenitization.

The aim here is to gain a more fundamental understanding of how the microfracture processes are affected by microstructural changes and impurity segregation during tempering. In this article, particular emphasis has been placed on studying microfracture processes at crack tips using an *in situ* technique developed first by Hong and Gurland.[7]

The material used in this study is an AISI 4340 steel whose nominal chemical composition is given in Table I. Heat treatments are austenitization at 1150 °C for 1 hour followed by quenching in agitated oil and tempering at 350 °C for 1 hour. This heat-treatment condition is known to be associated with TME, which is characterized by a trough in the plots of Charpy impact energy and plane strain fracture toughness as a function of tempering temperature (Figure 1).[8]

Direct observations of a crack opening process near a blunt notch tip were made using a specially designed wedge-loading stage, as shown in Figure 2(a). A thin double-cantilever beam (DCB) specimen (Figure 2(b)) was metallographically polished and specially etched by using a two-step etching technique to reveal prior austenite grain boundaries as well as basic tempered martensite structures. Prior austenite grain boundaries were clearly revealed using a hot sodium tridecylbenzene sulfonate etchant (100 ml of saturated aqueous picric acid with 1 g of sodium tridecylbenzene sulfonate). The etched specimen was then polished slightly without removing the prior austenite grain structure and etched again using nital etchant to observe simultaneously the morphology of carbides and other fine particles.

The microstructure of the 4340 steel tempered at 350 °C after 1150 °C austenitization consisted almost entirely of tempered martensite. The steel also contained inclusions, primarily manganese sulfides. The prior austenite grain size was approximately 200 μm. Banded structures with layers of a fine lath martensite region adjacent to more widely spaced layers of a twinned martensite region were preferentially aligned along the rolling direction, as shown in Figure 3.

Figures 4(a) through (f) are a series of micrographs showing the fracture initiation process at a blunt notch tip of the 4340 steel tempered at 350 °C after austenitization at 1150 °C. Figures 4(a) and (b) indicate that the morphology of tempered martensite is basically dislocated lath type with cementite carbides precipitated along the lath boundaries (interlath) and within the laths (intralath). At the initial stage of wedge loading, the shear bands were formed near the notch tip preferentially along the arrays of interlath cementite particles, as indicated by arrows in Figure 4(c). It was also observed that microcracks are formed at the prior austenite grain boundaries. These initial microcracks became larger in the direction normal to the wedge loading, producing intergranular discontinuous cracks. In the shear bands, the coarse MnS inclusions were ruptured first without affecting the subsequent main fracture path. When the wedge loading was continued, new localized shear bands were formed near the notch tip as the surrounding steel matrix underwent plastic deformation, eventually connecting to the notch tip (Figures 4(d) and (e)). The main

B.C. KIM, Research Assistant, S. LEE, Assistant Professor, D.Y. LEE, Associate Professor, and N.J. KIM, Associate Professor, are with the Department of Materials Science and Engineering, Pohang Institute of Science and Technology, Pohang 790-600, Korea.

Manuscript submitted September 18, 1990.

Table I. Chemical Composition (Weight Percent) of the AISI 4340 Steel Investigated

C	Mn	P	S	Si	Ni	Cr	Mo	Cu	V	Al	Ti	O
0.38	0.79	0.018	0.018	0.46	1.73	0.79	0.29	0.01	0.002	0.011	0.008	0.021

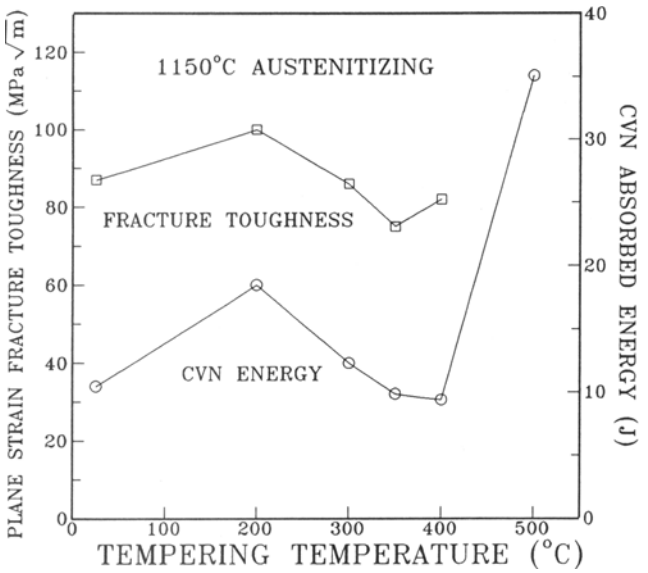

Fig. 1 — Room-temperature fracture toughnesses *vs* tempering temperature for an AISI 4340 steel.[8]

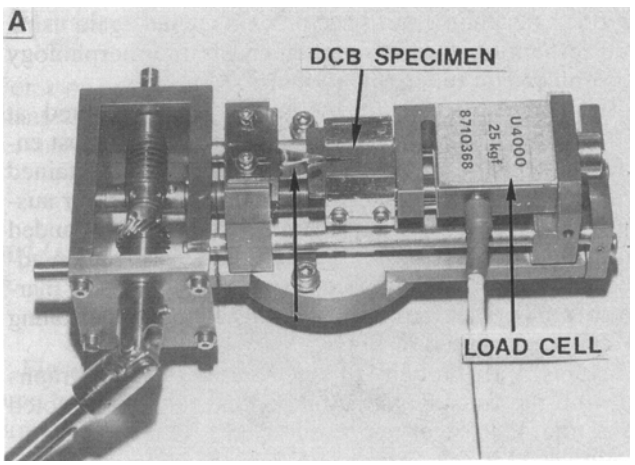

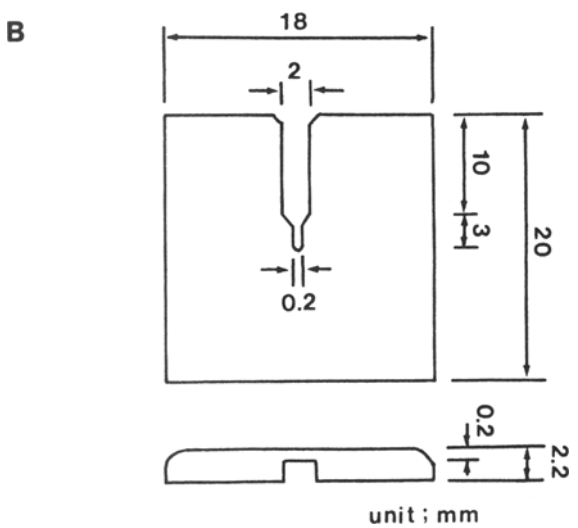

Fig. 2 — (*a*) The wedge loading stage used for *in situ* SEM observation which was inserted into the vacuum chamber of an SEM, replacing the standard sample stage. (*b*) The shape and dimensions of a thin DCB specimen (unit: millimeters).

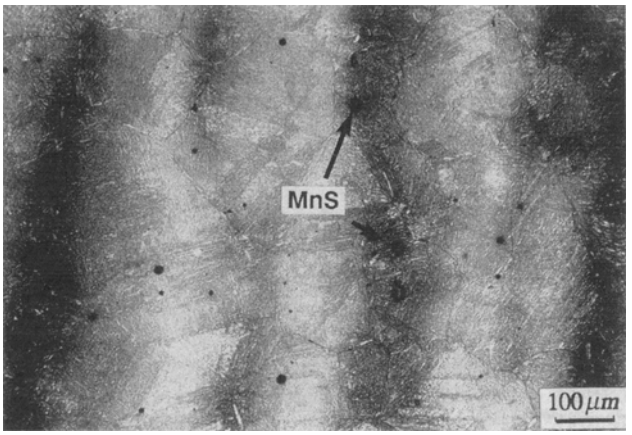

Fig. 3 — Optical micrograph of the 4340 steel austenitized at 1150 °C and tempered at 350 °C.

crack, therefore, proceeded along the localized shear band region to form a continuous crack (Figure 4(f)).

It is interesting to note from Figures 5(a) and (b) that when the main crack meets the intergranular discrete cracks associated with the prior austenite grain boundaries, the crack path is slightly deviated from the shear band, resulting in the intergranular fracture, as indicated by an arrow in Figure 5(a). When no adjacent intergranular discrete cracks exist around the main crack tip, however, the main crack follows along the localized shear bands (Figure 5(b)).

Figure 6 shows a typical scanning electron microscope (SEM) fractograph of these thin DCB specimens. It can be noted from Figure 6 that the fracture surface is entirely dominated by a transgranular ductile rupture mode without any evidence of intergranular fracture. This fracture surface contains two types of dimples: a set of large dimples that initiated at MnS inclusions and the other a set of smaller dimples distributed between the larger dimples that formed at cementite carbides. It has been found by Lee *et al.*[9] that the measured dimple spacings correlate well with the measured carbide particle spacings when the fracture mode is fibrous. Examination of the fracture surfaces in the SEM using energy-dispersive X-ray analysis (EDAX) indicates that the fracture surface area related to MnS inclusions is less than 10 pct of the total fracture surface area. Thus, it is clear that void initiation at cementite particles is the dominant fracture initiation mechanism. A significant amount of long elongated dimples was also detected and found to be lined up, as indicated by arrows in Figure 6. Even though the direction of the lath boundaries in Figure 4(b) could not be identified, these elongated dimples are probably due to the platelike interlath cementite carbides. This observation supports the explanation that the formation of cementite particles during 350 °C tempering plays an important role in the fracture process associated with TME, as suggested by Thomas and co-workers.[1,3]

From the fractographic results and the *in situ* fracture observation, the fracture mechanism associated with TME can be explained as follows. At the relatively low stress levels, microcracks form at the weakened prior austenite

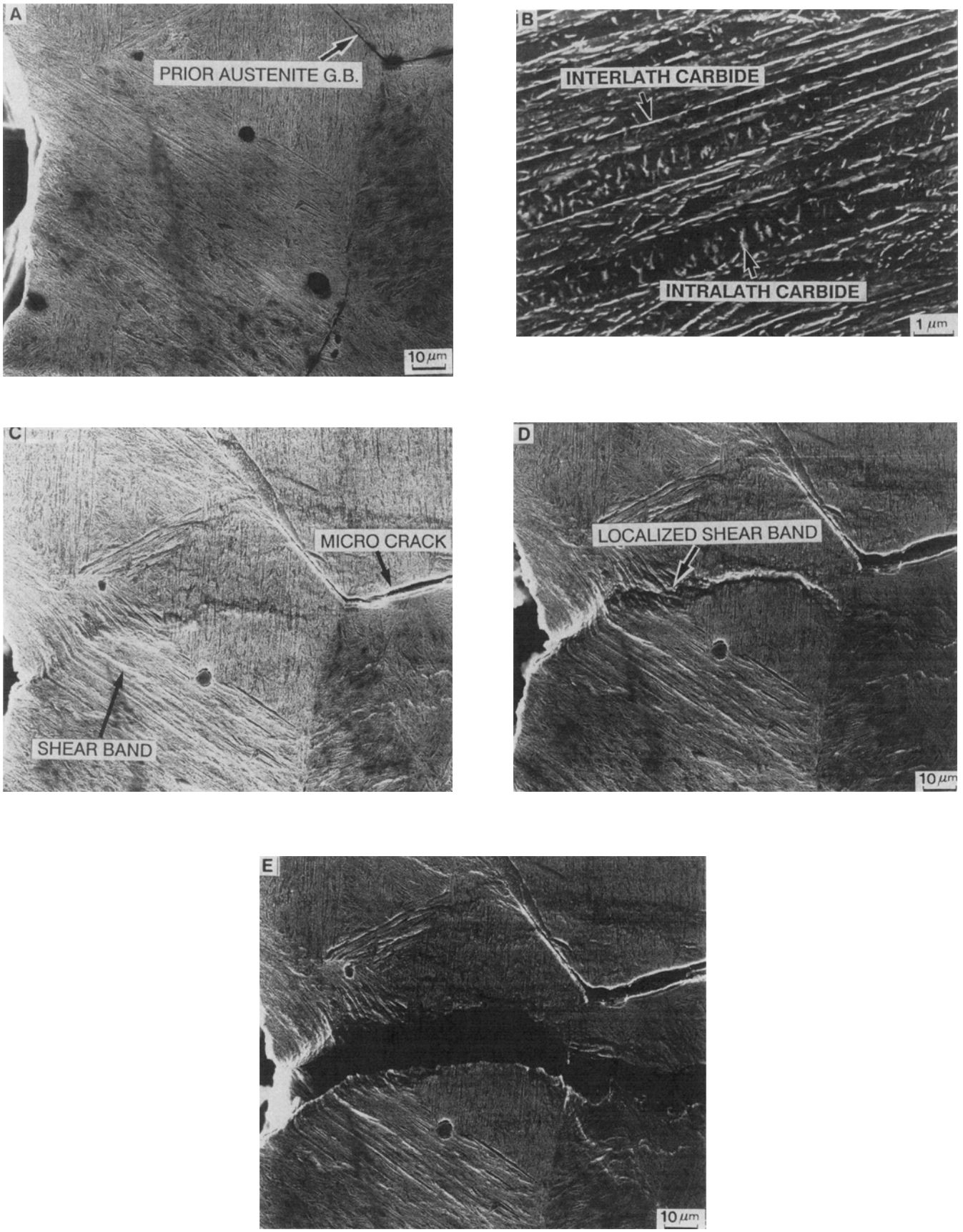

Fig. 4—A series of SEM micrographs of the near blunt notch tip in the 4340 steel quenched from 1150 °C followed by tempering at 350 °C: (*a*) and (*b*) notch profile and microstructure before loading, (*c*) shear band formation along interlath cementite particles (arrows) and microcracking at prior austenite grain boundaries, and (*d*) and (*e*) eventual crack propagation path along the localized shear bands.

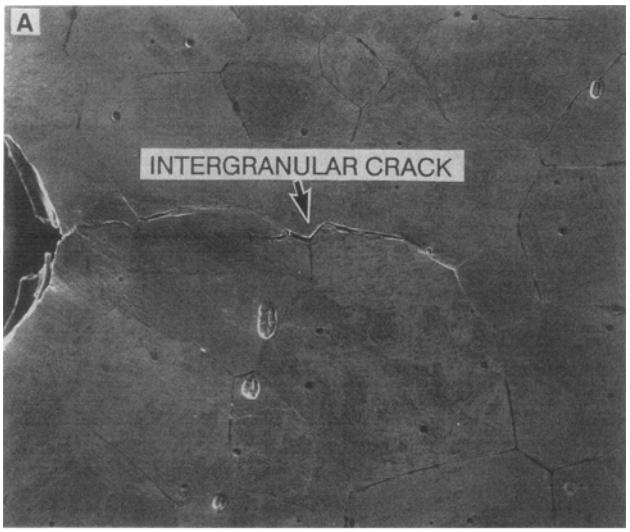

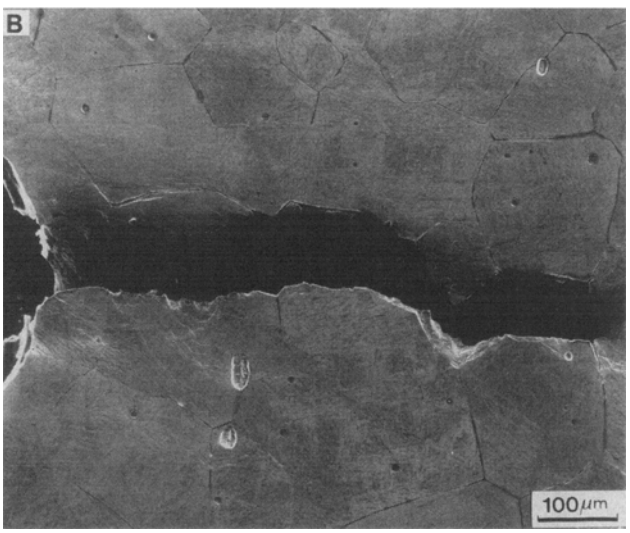

Fig. 5—(*a*) and (*b*) Crack initiation and growth processes of the 4340 steel subjected to the TME condition, showing the crack path partly deviated from the localized shear band to cause intergranular fracture.

grain boundaries. In addition to these microcracks, the deformation becomes localized into intense shear bands along platelike interlath carbides. Since the high strains within the shear bands can also cause microvoids to form at the carbide-matrix interfaces, voids will form around

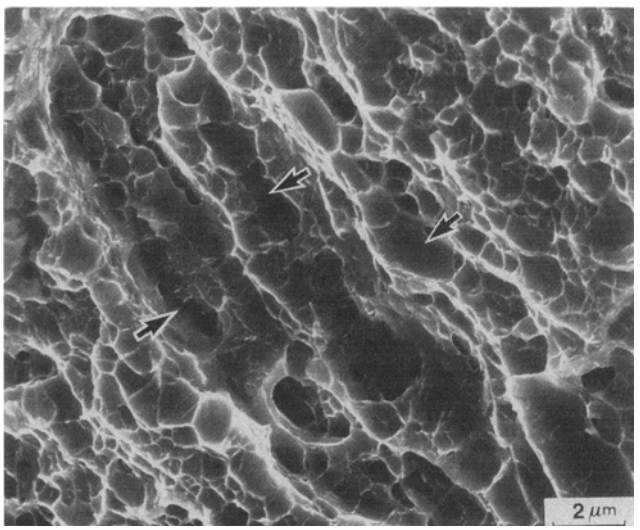

Fig. 6—SEM fractograph of the fractured thin DCB specimen of the 4340 steel quenched from 1150 °C followed by tempering at 350 °C.

these carbides within the shear bands, and failure will occur along these shear bands in a ductile manner. Direct observations of the crack initiation in the 4340 steel suggest that the presence of carbide particles strongly influences the fracture initiation process. Therefore, the decrease in toughness induced by tempering at 350 °C is mainly attributed to the precipitation of cementite particles.

REFERENCES

1. G. Thomas: *Metall. Trans. A*, 1978, vol. 9A, pp. 439-50.
2. R.M. Horn and Robert O. Ritchie: *Metall. Trans. A*, 1978, vol. 9A, pp. 1039-53.
3. M. Sarikaya, B.G. Steinberg, and G. Thomas: *Metall. Trans. A*, 1982, vol. 13A, pp. 2227-37.
4. S.K. Banerji, C.J. McMahon, Jr., and H.C. Feng: *Metall. Trans. A*, 1978, vol. 9A, pp. 237-47.
5. C.L. Briant and S.K. Banerji: *Int. Met. Rev.*, 1978, no. 4, pp. 164-99.
6. F. Zia-Ebrahimi and G. Krauss: *Acta Metall.*, 1984, vol. 10, pp. 1767-77.
7. J. Hong and J. Gurland: *Metallography*, 1981, vol. 14, pp. 225-36.
8. S. Lee, D.Y. Lee, and R.J. Asaro: *Metall. Trans. A*, 1989, vol. 20A, pp. 1089-1103.
9. S. Lee, L. Majno, and R.J. Asaro: *Metall. Trans. A*, 1985, vol. 16A, pp. 1633-48.